

Dispersive Media Subcell Averaging in the FDTD Method using Corrective Surface Currents

Joachim Hamm, Fabian Renn, and Ortwin Hess

Abstract—We present a corrective subcell averaging technique that improves on the accuracy of the volume-averaged finite-difference time-domain (FDTD) method in the presence of dispersive material interfaces. The method is based on an alternative effective-medium formulation that captures field discontinuities at interfaces as electric and magnetic surface currents. In calculating the spectra of strongly dispersive Mie scatterers we demonstrate that the derived FDTD algorithm is both highly efficient and able to approximately restore second order accuracy.

I. INTRODUCTION

Half a century after its invention by Kane Yee [1] the finite-difference time-domain (FDTD) method remains a popular choice for simulating the propagation of electromagnetic waves and their interaction with electronic media [1], [2]. The simplicity of the algorithm and its low computational footprint are contrasted by the use of non-conformal grids, which, if field discontinuities are not properly accounted for, reduce accuracy from second to first order [3], [2]. This not only negates the advantage of the staggered grid Yee-algorithm but also severely impacts on the computational cost when modeling systems that exhibit geometric features on sub-wavelength scales.

The problem of restoring accuracy of the FDTD scheme in the presence of interfaces was first studied in the microwave regime [4], [5], [6]. Since then a variety of effective-permittivity (EP) models have been suggested for the treatment of field discontinuities at material interfaces, which can broadly be classified as either counter-path (CP) or volume-polarized (VP) models [7], [8], [9], [4]. Of particular importance for this work is the VP model proposed by Farjadpour et al [10]. Based on the continuity of the $\mathbf{E}_{||}$ and \mathbf{D}_{\perp} field components the volume-integrated permittivity tensor is derived as $\epsilon_{\infty}^{-1} = \langle \epsilon_{\infty}^{-1} \rangle \mathbf{P} + \langle \epsilon_{\infty} \rangle^{-1} (1 - \mathbf{P})$, where $\mathbf{P} = \mathbf{n} \otimes \mathbf{n}$ performs a vector-projection onto the face-normal of the interface. The application of this non-diagonal permittivity tensor requires interpolation of the Yee-centered \mathbf{D} field to the cell-center and subsequent interpolation of the cell-centered \mathbf{E} field back onto the Yee-grid, a procedure that effectively equates to a smoothing operation with extended spatial stencil. Nonetheless, as numerical evidence suggests, the spectral accuracy increases to approximately second order, reducing the computational cost for problems that involve non-dispersive dielectrics (e.g., photonic crystal applications). In 2007, Deinega et al [11] suggested an approach that extends this method to the linear dispersive regime. Their algorithm uses the decomposition $\mathbf{E} = \mathbf{E}_{||} + \mathbf{n}(E_{\perp,1} + E_{\perp,2})$ to split the electric field into four components, which drive the polarization currents at the interface. A recent work by Liu

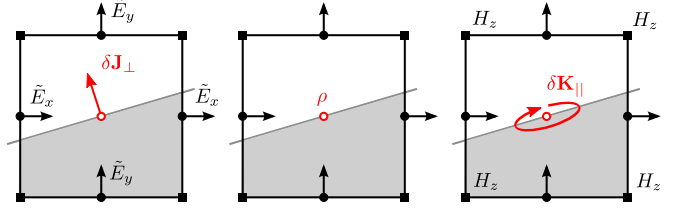


Figure 1. (color online) Schematic of the VA+CC FDTD algorithm. $\tilde{\mathbf{E}}$ and \mathbf{H} fields (black) are calculated using the standard VA FDTD algorithm, introducing systematic errors at interface-cells due to discontinuities of the field. The surface currents $\delta \mathbf{J}_{\perp}$ and $\delta \mathbf{K}_{||}$ (red) correct the errors during the electric (left) and magnetic (right) update steps. Calculating the corrective currents requires an intermediate step for integrating the surface charge density ρ at the cell center (middle). The algorithm is compatible with the standard Yee scheme as the corrections only apply to interface cells.

et al [12] shows that, in case of dielectric-dispersive media boundaries, one does not need to split the normal field as long as one can formulate a modified effective polarization response for the normal component. The resulting algorithm is less general yet computationally more efficient. However, as in [11], it remains unspecified how the algorithm interfaces with the standard Yee-algorithm that could be efficiently employed across regions where permittivities are smooth.

Here, we present an alternative approach (see Fig. 1) that solves the EP curl equations on the Yee-grid using the standard volume-averaged (VA) FDTD algorithm but replaces the electric field with an approximate field $\tilde{\mathbf{E}}$ that is continuous across non-dispersive interfaces. The field discontinuities at dispersive media interfaces need then to be captured as corrective electric and magnetic currents $\delta \mathbf{J}_{\perp}$ and $\delta \mathbf{K}_{||}$, which are induced by a surface charge field ρ . Based on this idea we first formulate an effective medium theory and then show how this EP model translates into a FDTD scheme that offers some unique advantages: 1) the algorithm naturally extends the standard FDTD scheme by introducing additive current corrections that only apply at interface cells; 2) only the normal field components are subjected to spatial smoothing operations at the interface; and 3) calculating the corrections is computationally efficient and requires no alteration of the dispersive response functionals (as for example in [12]). In the result section, we apply the derived algorithm to the example of a highly dispersive Mie scatterer in two-dimensions, demonstrating stability and allowing for a comparison of numerical errors between the VA+CC (using current corrections), the VA, and standard staircasing schemes.

II. CORRECTIVE-CURRENT SUBCELL SMOOTHING

Our starting point are the split-field equations derived by Deinega et al [11] (equations (3)-(6) therein). Without loss of

generality we write the scalar permittivity as $\varepsilon(\omega) = \varepsilon_\infty + \chi(\omega)$ and transform the equations into time-domain. Using a slightly different notation, we write

$$\begin{aligned} \langle \varepsilon_\infty \rangle \partial_t \mathbf{E}_{||} &= [\nabla \times \mathbf{H}]_{||} - f_1 \mathbf{J}_1[\mathbf{E}_{||}] - f_2 \mathbf{J}_2[\mathbf{E}_{||}] \\ \varepsilon_{\infty,1} \partial_t E_{\perp,1} &= f_1 [\nabla \times \mathbf{H}]_{\perp} - J_1[E_{\perp,1}] \\ \varepsilon_{\infty,2} \partial_t E_{\perp,2} &= f_2 [\nabla \times \mathbf{H}]_{\perp} - J_2[E_{\perp,2}] \end{aligned} \quad (1)$$

where $\mathbf{J}_{1/2} = \partial_t \mathbf{P}_{1/2}$ are functionals of \mathbf{E} , describing the (isotropic) polarization current response. The symbols ' \perp ' and ' $||$ ' denote vector-projections relative to the interface with face-normal \mathbf{n} and the notation $J_{1/2} = \mathbf{n} \cdot \mathbf{J}_{1/2}$ is introduced for brevity. This formulation of Ampère's law implicitly assumes an averaging over a volume-cell that is intersected by a boundary between media 1 and 2 with cell-filling ratios f_1 and f_2 ($f_1 + f_2 = 1$). Angled brackets are used throughout this work to denote volume averages of the form $\langle \varepsilon_\infty \rangle = f_1 \varepsilon_{\infty,1} + f_2 \varepsilon_{\infty,2}$.

The derivation of (1) is straightforward but their translation into an efficient and stable finite-difference scheme is not. To retain second order accuracy, the field components in the curl expression $\nabla \times \mathbf{H}$ should be calculated on the Yee-grid while the projections onto parallel and normal projections require interpolation to the cell-center. After calculating the updates of the $\mathbf{E}_{||}$, $E_{\perp,1}$ and $E_{\perp,2}$ components at the cell-center the \mathbf{E} -field thus needs to be reconstructed and redistributed onto the Yee-grid. However, a direct implementation proves impractical for the following reason. The cell-centered four-field representation and the extended spatial stencil (due to interpolation between the grids) fundamentally differs from the standard Yee-algorithm. As a consequence the algorithm is deployed across the whole grid irrespective of whether cells are intersected by media-boundaries or not. This introduces unnecessary smoothing operations across the whole grid, increases the computational cost and requires re-implementing the infrastructure typically associated with FDTD frameworks (e.g., total-field scattered-field injection, boundary conditions etc).

We therefore seek to derive an alternative formulation where the standard Yee scheme can be efficiently applied across the domain augmented by corrections that only apply to the comparably small number of interface cells. The basis for this corrective method is a reformulation of (1). In introducing new variables for the normal electric field and the density of the induced surface charges,

$$\begin{aligned} E_{\perp} &= E_{\perp,1} + E_{\perp,2} \\ \rho &= f_2 \varepsilon_{\infty,1} E_{\perp,1} - f_1 \varepsilon_{\infty,2} E_{\perp,2} \end{aligned} \quad (2)$$

Equation (1) can be cast into the form

$$\begin{aligned} \langle \varepsilon_\infty \rangle \partial_t \mathbf{E}_{||} &= [\nabla \times \mathbf{H}]_{||} - f_1 \mathbf{J}_1[\mathbf{E}_{||}] - f_2 \mathbf{J}_2[\mathbf{E}_{||}] \\ \langle \varepsilon_\infty^{-1} \rangle^{-1} \partial_t E_{\perp} &= [\nabla \times \mathbf{H}]_{\perp} - \zeta_1 J_1[E_{\perp,1}] - \zeta_2 J_2[E_{\perp,2}] \\ \partial_t \rho &= f_1 J_2[E_{\perp,2}] - f_2 J_1[E_{\perp,1}] \end{aligned} \quad (3)$$

with $\zeta_{1/2} = \langle \varepsilon_\infty^{-1} \rangle^{-1} \varepsilon_{\infty,1/2}^{-1}$. The fact that $\langle \varepsilon_\infty \rangle^{-1} \neq \langle \varepsilon_\infty^{-1} \rangle$ makes it impossible to reconstruct Ampère's law for the discretized (i.e., volume averaged) electric field by adding the first two equations. However, we can define an approximate

electric field

$$\tilde{\mathbf{E}} = \mathbf{E}_{||} + \langle \varepsilon_\infty \rangle^{-1} \langle \varepsilon_\infty^{-1} \rangle^{-1} \mathbf{n} E_{\perp} \quad (4)$$

which, in the absence of dispersive currents, is continuous across material interfaces and matches \mathbf{E} at non-interface cells. Combining the first two equations of (3) in this fashion yields

$$\langle \varepsilon_\infty \rangle \partial_t \tilde{\mathbf{E}} = \nabla \times \mathbf{H} - \langle \mathbf{J}[\tilde{\mathbf{E}}] \rangle - \delta \mathbf{J}_{\perp} \quad (5)$$

We note that apart from the extra current term $\delta \mathbf{J}_{\perp}$ we now have recovered the volume-averaged curl equation for the electric field. The correction $\delta \mathbf{J}_{\perp} = \mathbf{n} \delta J_{\perp}$ compensates the error that arises from using volume-averaged permittivities and current densities for the normal components. Assuming an isotropic response one obtains after some algebra

$$\delta J_{\perp} = -f_1 J_1[\tilde{\mathbf{E}}] - f_2 J_2[\tilde{\mathbf{E}}] + \zeta_1 J_1[E_{\perp,1}] + \zeta_2 J_2[E_{\perp,2}] \quad (6)$$

for the surface current correction. Its calculation requires the scalar fields $E_{\perp,1/2}$ that are obtained by projection

$$\begin{aligned} E_{\perp,1} &= f_1 \varepsilon_{\infty,1}^{-1} (\langle \varepsilon_\infty \rangle \mathbf{n} \cdot \tilde{\mathbf{E}} + f_1^{-1} \zeta_2 \rho) \\ E_{\perp,2} &= f_2 \varepsilon_{\infty,2}^{-1} (\langle \varepsilon_\infty \rangle \mathbf{n} \cdot \tilde{\mathbf{E}} - f_2^{-1} \zeta_1 \rho) \end{aligned} \quad (7)$$

Inserting these relations into (6) yields

$$\delta J_{\perp} = f_1 (J_1^*[\tilde{\mathbf{E}}, \rho] - J_1[\tilde{\mathbf{E}}]) + f_2 (J_2^*[\tilde{\mathbf{E}}, \rho] - J_2[\tilde{\mathbf{E}}]) \quad (8)$$

where we defined

$$J_{1/2}^*[\tilde{\mathbf{E}}, \rho] = \zeta_{1/2} \varepsilon_{\infty,1/2}^{-1} (\langle \varepsilon_\infty \rangle J_{1/2}[\tilde{\mathbf{E}}] \pm f_{1/2}^{-1} \zeta_{2/1} J_{1/2}[\rho]) \quad (9)$$

This implies that the electric current correction can be calculated from the currents induced by $\tilde{\mathbf{E}}$ and ρ . The terms in (8) proportional to $J_{1/2}[\tilde{\mathbf{E}}]$ are the volume-averaged normal currents, which need to be subtracted from eq. (5) before adding the correct $J_{1/2}^*[\tilde{\mathbf{E}}, \rho]$ contributions. Applying (7) to the equation for the charge field ρ [see (3)] gives

$$(f_1 f_2)^{-1} \partial_t \rho = \zeta_2^{-1} J_2^*[\tilde{\mathbf{E}}, \rho] - \zeta_1^{-1} J_1^*[\tilde{\mathbf{E}}, \rho] \quad (10)$$

In order to complete the update of the magnetic field the correct electric field \mathbf{E} needs to be recovered from $\tilde{\mathbf{E}}$. This is achieved by introducing a corrective magnetic current density

$$\begin{aligned} \delta \mathbf{K}_{||} &= \nabla \times \mathbf{n} \delta E_{\perp} \\ &= \nabla \times \mathbf{n} (\langle \varepsilon_\infty^{-1} \rangle \langle \varepsilon_\infty \rangle - 1) \mathbf{n} \cdot \tilde{\mathbf{E}} \end{aligned} \quad (11)$$

to Faraday's law

$$\partial_t \mathbf{H} = -\nabla \times \tilde{\mathbf{E}} - \delta \mathbf{K}_{||} \quad (12)$$

rendering the overall scheme bi-isotropic. This completes our reformulation of the effective cell-averaged Maxwell's equations. The curl equations (5), (12) together with the electric and magnetic current corrections (8) and (11) and the surface charge equation (10) form a closed set of equations. We achieved our goal of finding an effective medium formulation where corrective current densities $\delta \mathbf{J}_{\perp}$ and $\delta \mathbf{K}_{||}$ apply at interface cells and vanish whenever permittivities vary smoothly across cells. The magnetic current correction $\delta \mathbf{K}_{||}$ accounts for field discontinuities caused by a jump in the static permittivity across the interface, while the electric current correction $\delta \mathbf{J}_{\perp}$ captures all discontinuities induced

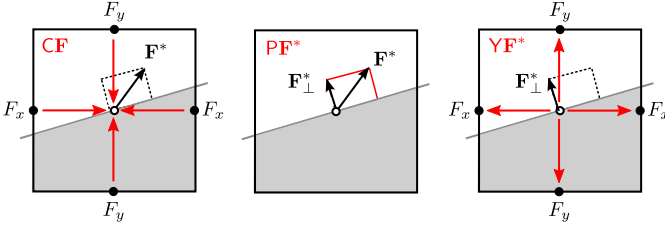


Figure 2. (color online) Pictorial representation of the action of the C, P and Y operators. C interpolates the vector of Yee-centered components \mathbf{F} to the cell-centered vector \mathbf{F}^* (left), P projects a cell-centered vector onto the face normal (center), and Y interpolates a cell-centered vector back onto the Yee-grid (right).

by the dispersive material response. Notably, calculating the induced corrections requires only three additional physical fields, namely the interface charge field ρ and the associated induced normal currents $J_{1/2}[\rho]$.

III. YEE-COMPATIBLE CORRECTIVE-CURRENT FDTD SCHEME

We now proceed to translate the equations derived in the previous section into a versatile and efficient FDTD scheme. In compliancy with the standard Yee-scheme we integrate (5) and (12) in two distinct half-steps by first performing the electric field update

$$\begin{aligned} \tilde{\mathbf{E}}^{n+1/2} = & \tilde{\mathbf{E}}^{n-1/2} + \Delta t \langle \varepsilon_\infty \rangle^{-1} \nabla \times \mathbf{H}^n \\ & - \Delta t \langle \varepsilon_\infty \rangle^{-1} (\langle \mathbf{J}^n [\tilde{\mathbf{E}}^{n-1/2}] \rangle + \delta \mathbf{J}_\perp^n) \end{aligned} \quad (13)$$

and then the magnetic field update

$$\mathbf{H}^{n+1} = \mathbf{H}^n - \Delta t (\nabla \times \tilde{\mathbf{E}}^{n+1/2}) + \Delta t \delta \mathbf{K}_\parallel^{n+1/2} \quad (14)$$

To shorten the notation, we implicitly assume that $\tilde{\mathbf{E}}^{n+1/2}$ and \mathbf{H}^n are $3N$ -dimensional vectors (N being the number of Yee-cells) aggregating the electric and magnetic field components on the staggered subgrids across the problem domain. In this formulation the curl-operator $\nabla \times$ is a matrix that performs a stencil operation at each point of either the electric or magnetic subgrid. The permittivity tensor $\langle \varepsilon_\infty \rangle^{-1}$ is a diagonal matrix that can be precalculated by volume-averaging the permittivities at the various positions of the Yee-cube. In a similar way $\langle \mathbf{J}^n [\tilde{\mathbf{E}}^{n-1/2}] \rangle$ can be obtained by weighting the contributing current vectors \mathbf{J}_i^n with the matrix of precalculated cell-filling factors f_i . It is important to note that the treatment of dispersive currents requires a preceding evaluation of the response functionals $\mathbf{J}_i^n[\dots]$, by either integrating appropriate auxiliary differential equations (e.g., for the Lorentz pole) [2] or by using the piecewise linear recursive convolution (PLRC) method [13].

Following the arguments laid out in the previous section it is clear that the corrective currents $\delta \mathbf{J}_\perp^n$ and $\delta \mathbf{K}_\parallel^{n+1/2}$ vanish whenever the material constants vary smoothly across cells. For these volume cells $\tilde{\mathbf{E}} \rightarrow \mathbf{E}$ and the update equations reduce themselves to the dispersive VA FDTD method, which, as $\langle \varepsilon_\infty \rangle^{-1}$ is diagonal can be efficiently integrated using the standard Yee-scheme. Within interface cells, on the other hand, $\tilde{\mathbf{E}}$ differs from the electric field \mathbf{E} and a corrective step is

necessary to accurately account for the discontinuity of the normal field component. As shown before the discontinuity in the normal component is directly proportional to the surface charge density ρ induced at the interface. Discretizing (10) results in an update equation for ρ

$$\rho^{n+1/2} = \rho^{n-1/2} + \Delta t (f_1 f_2) (\zeta_2^{-1} J_2^{*n} - \zeta_1^{-1} J_1^{*n}) \quad (15)$$

that requires evaluation of the currents $J_{1/2}^{*n}$ according to (9). In difference to the electromagnetic field components, which are evaluated on the Yee-grid, ρ is a cell-centered quantity. We therefore need to introduce operators to interpolate between the Yee- and cell-centered grids. Figure 2 illustrates the action of the Y and C interpolation operators (left and right panel) together with the projection operator P (center panel). Applied to write (9) this yields

$$\begin{aligned} J_{1/2}^{*n} = & \zeta_{1/2} \varepsilon_{\infty,1/2}^{-1} (\text{PC} \langle \varepsilon_\infty \rangle \mathbf{J}_{1/2}^n [\tilde{\mathbf{E}}^{n-1/2}] \\ & \pm f_{1/2}^{-1} \zeta_{2/1} J_{1/2}^n [\rho^{n-1/2}]) \end{aligned} \quad (16)$$

This expression recycles the previously calculated $\mathbf{J}_{1/2}^n$ currents on the Yee-grid but introduces a charge-current $J_{1/2}^n[\rho^{n-1/2}]$ that, using the same current-functional, is evaluated at the cell center. To improve smoothness of the fields under the projection/interpolation operation we multiply $\mathbf{J}_{1/2}^n$ with the $\langle \varepsilon_\infty \rangle$ tensor, which is already available on the Yee-grid. In contrast, the coefficients $\zeta_{1/2}$, $\varepsilon_{\infty,1/2}^{-1}$ and $f_{1/2}^{-1}$ and the face-normal \mathbf{n} are parameters that are defined at the cell-center (see Fig. 8). As (16) can be evaluated on-the-fly, the only additional physical fields that need to be stored at the cell-center are ρ and its induced currents $J_{1/2}^n[\rho^{n-1/2}]$.

With the surface charge and its currents known, it becomes possible to compute the corrections $\delta \mathbf{J}_\perp^n$ and $\delta \mathbf{K}_\parallel^{n+1/2}$ that enter the update equations (13) and (14). However, the order of operators (and hence the discretization) is ambiguous, and, as the scheme is corrective, can impact on the stability of the scheme. A numerical analysis of the computational errors suggests that $\mathbf{J}_{1/2}^n$ is best multiplied with the $\langle \varepsilon_\infty \rangle$ tensor before centering to the grid. This is due to the fact that the normal component of $\langle \varepsilon_\infty \rangle \tilde{\mathbf{E}}$ retains smoothness across adjacent cells with different ε_∞ . Further, to maintain consistency between the Yee and cell-centered update equations (13), (14) and (15) we assign parameters as indicated by Fig. 8. This allows us to write

$$\begin{aligned} \langle \varepsilon_\infty \rangle^{-1} \delta \mathbf{J}_\perp^n = & - \langle \varepsilon_\infty \rangle^{-2} (f_1 \text{YPC} \langle \varepsilon_\infty \rangle \mathbf{J}_1^n - f_2 \text{YPC} \langle \varepsilon_\infty \rangle \mathbf{J}_2^n \\ & + \mathbf{Yn} f_1 J_1^{*n} + \mathbf{Yn} f_2 J_2^{*n}) \end{aligned} \quad (17)$$

where volume filling factors in the first line are applied after centering onto the Yee-grid, and, for the second line, directly at the cell-center.

The discretization of the magnetic current requires both terms in (11) to be interpolated to the center before spreading them out again onto the Yee-grid. We obtain

$$\delta \mathbf{K}_\parallel^{n+1/2} = \nabla \times \delta \tilde{\mathbf{E}}_\perp^{n+1/2} \quad (18)$$

with

$$\delta \tilde{\mathbf{E}}_\perp^{n+1/2} = (\mathbf{Y} \langle \varepsilon_\infty^{-1} \rangle - \langle \varepsilon_\infty \rangle^{-1} \mathbf{Y}) \text{PC} \langle \varepsilon_\infty \rangle \tilde{\mathbf{E}}^{n+1/2} \quad (19)$$

Algorithm 1 Sequence of field updates (VA+CC)

- $n+1/2$ (on Yee-grid):
 - VA: update $\tilde{\mathbf{E}}^{n-1/2} \rightarrow \tilde{\mathbf{E}}^{n+1/2}$ w/o $\delta\mathbf{J}_\perp^n$ [(13)]
 - CC: add correction $\delta\mathbf{J}_\perp^n$ [(17)]
 - $n+1/2$ (on centered-grid):
 - CC: update $\rho^{n-1/2} \rightarrow \rho^{n+1/2}$ [(15)]
 - CC: evaluate $J_i^{n+1}[\rho^{n+1/2}]$ (for next cycle)
 - $n+1$ (on Yee-grid)
 - VA: evaluate $\mathbf{J}_i^{n+1}[\tilde{\mathbf{E}}^{n+1/2}]$ (for next cycle)
 - VA: update $\mathbf{H}^n \rightarrow \mathbf{H}^{n+1}$ w/o $\delta\mathbf{K}_\parallel^{n+1/2}$ [(14)]
 - CC: add correction $\delta\mathbf{K}_\parallel^{n+1/2}$ [(18)]
-

Fundamentally, both the electric and magnetic current corrections can be calculated on-the-fly. As the corrections only apply to interface cells, they can be added in a separate step to the update equations. This means that the update equations of the VA FDTD scheme can be deployed across the whole grid, followed by oversampling steps that perform the current-corrections (CC) for interface cells only. The complete update sequence for the VA+CC algorithm is shown in Alg. 1.

As each step can be associated with a loop over cells, it becomes evident that the current-correction (CC) steps augment those related to the VA FDTD scheme. As the CC steps only apply to interface cells, the computational overhead of the VA+CC FDTD scheme is not significant unless the number of interface cells becomes comparable to the number of volume cells.

IV. RESULTS

To verify the accuracy of our method we compare our numerical calculations with the Mie scattering cross section of an infinitely extended strongly dispersive cylinder excited by a TM plane-wave. The dielectric function describing the response of the cylinder consists of a single Lorentzian resonance at $\lambda_0^{-1} = 0.25R$ and a background dielectric constant of $\varepsilon_\infty = 4$, where R is the radius of the cylinder. Figure 3a shows real and imaginary parts of the complex permittivity $\varepsilon(\lambda^{-1}) = \varepsilon'(\lambda^{-1}) + i\varepsilon''(\lambda^{-1}) = \varepsilon_\infty + 2.5\lambda_0^{-2}(\lambda_0^{-2} - \lambda^{-2} - i0.05\pi^{-1}\lambda^{-1})^{-1}$ together with the analytically calculated scattering cross-sections for scatterers with and without the dispersive contribution $\chi(\lambda^{-1})$ (Fig. 3b).

The numerical setup of the 2D calculation is depicted in Fig. 4. An incident field is injected into the system at one of the boundaries of a standard Total-Field-Scattered-Field (TFSF) box [2]. The energy flux $\mathbf{E} \times \mathbf{H}$ of the scattered field is then recorded at the boundary of a box located outside of the TFSF box. The computational region is terminated with perfectly matched layers (PML) [2] which nearly completely attenuate any reflections caused by the computational boundary. After the simulation, the scattering spectrum can be recovered by Fourier-transforming the recorded energy flux.

Figure 5 (top) shows the difference between the analytic and numerical scattering cross sections obtained by numerical simulation with a resolution of eight Yee-cells per cylinder radius. The results of the VA+CC FDTD scheme (dashed red

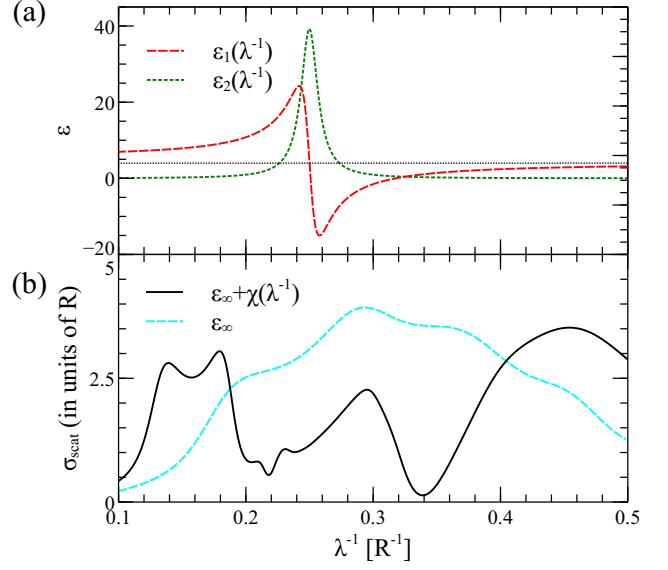


Figure 3. (color online) (a) the real (dashed) and imaginary (dotted) part of the dielectric function of an infinitely long cylinder and (b) the analytically calculated scattering cross section (solid). The dotted curve in (b) represents the scattering cross section of a cylinder with a purely static dielectric constant of $\varepsilon_\infty = 4$ (indicated by the thin dotted line in (a))

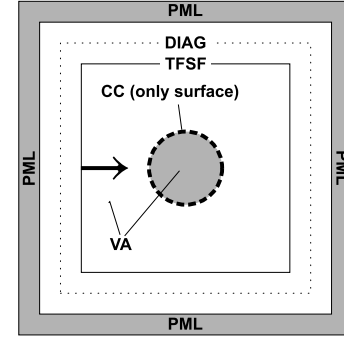


Figure 4. Computational setup: an incident pulse is injected on the inner left boundary of a TFSF box. The pulse interacts with the scatterer and leaves the TFSF box outside of which the energy flux of the scattered field is recorded (dotted line marked “DIAG”). The boundary of the computational region is terminated with perfectly matched layers (PML). The current corrections (CC) $\delta\mathbf{J}_\perp$ and $\delta\mathbf{K}_\parallel$ are only applied at the surface of the cylinder (thick dashed line).

line) are in better agreement with the analytical calculation than the VA FDTD scheme (dotted green line) throughout the spectrum. For comparison, the result of a simple staircased FDTD scheme was included in the figure (dash-dotted blue line). By selectively disabling either the current correction $\delta\mathbf{J}_\perp$ or $\delta\mathbf{K}_\parallel$ and subtracting the result from the VA FDTD scheme, the contributions of the charge corrections to the spectrum were quantified (Fig. 5b). The contribution of $\delta\mathbf{K}_\parallel$ is significant in the entire recorded spectral range, while, the contribution of $\delta\mathbf{J}_\perp$ shows a peak at a frequency which is slightly offset to the resonance frequency of the Lorentzian (indicated by the vertical dotted line). To illustrate the spatial dependence of the corrections and the charge density we plot contour images of the charge field ρ (Fig. 6b), the energy density of the electric correction $\delta\mathbf{J}_\perp \cdot \mathbf{E}$ (Fig. 6c), and the

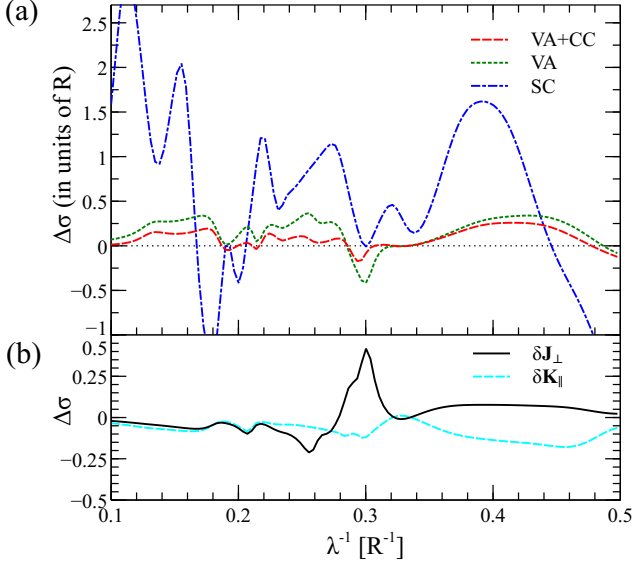


Figure 5. (color online) (a) difference between the analytic and numerical scattering cross section spectrum of an infinitely long dispersive Mie cylinder calculated with a VA FDTD scheme with (red dashed) and without (green dotted) charge corrections. The result of a staircased FDTD scheme is shown for reference (dashed-dotted blue). The thin dotted black horizontal line is a guide to the eye. (b) the contribution of the individual charge corrections to the cross section spectrum

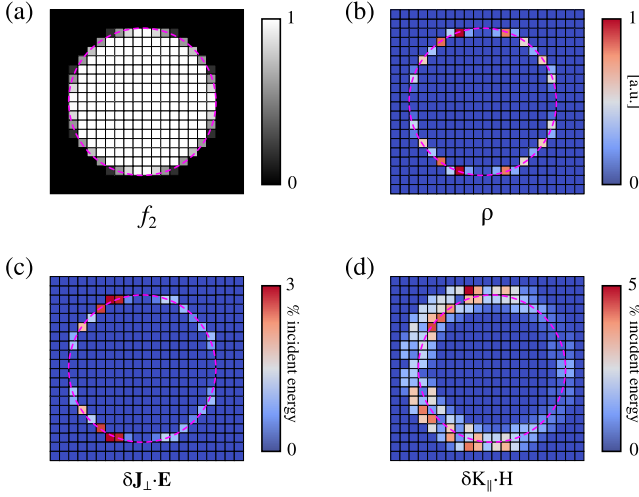


Figure 6. (color online) snapshot of (a) the volume filling factor f_2 of the interface cells (b) the charge field ρ (c) the electric current correction energy $\delta J_{\perp} \cdot E$ (d) the magnetic current correction energy $\delta K_{\parallel} \cdot H$.

energy density of the magnetic correction $\delta K_{\parallel} \cdot H$ (Fig. 6d). Whereas the corrections associated with the charge density and electric field correction are stored at the cell center, the correction associated with $\delta K_{\parallel} \cdot H$ is calculated from Yee-centered quantities and therefore appears to be smeared out over several adjacent cells.

To investigate the convergence behavior of the charge correction algorithm, numerical simulations with increasing resolution N were conducted. The RMS error for each simulation was obtained, by comparing the numerical scattering cross section spectrum with the analytical result (Fig. 7a). The VA (green diamonds) and the staircasing (blue circles) FDTD

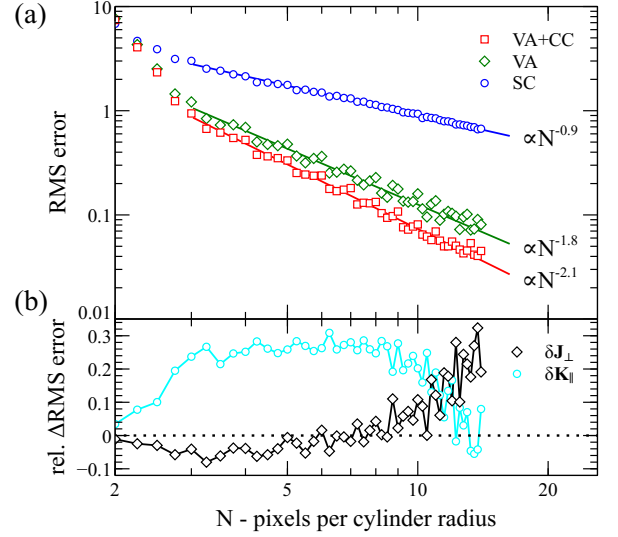


Figure 7. (color online) RMS error vs. increasing pixels per cylinder radius N . (a) the RMS error of staircasing (blue circles), VA (green diamonds) and VA+CC FDTD (red squares) schemes. (b) the relative change in error when enabling either the δJ_{\perp} (cyan circles) or δK_{\parallel} (black diamonds) current correction compared to the VA FDTD scheme error.

scheme produce errors that are significantly larger than those of the VA+CC scheme (red squares), which shows a decrease of error proportional to $\propto N^{-2.1}$. This means that for this particular system VA+CC achieves an accuracy that exceeds second order.

The overall error reduction is achieved by the combined action of the corrections δJ_{\perp} and δK_{\parallel} . To quantify their impact, we isolate their contributions to the error reduction as shown in the lower graph of Fig. 7. For low resolutions (smaller than ≈ 10 pixels per cylinder radius) the charge correction δK_{\parallel} is dominant in reducing the error. In this resolution regime, volume averaging of the static dielectric constant $\langle \epsilon_{\infty} \rangle$ for the perpendicular electric field component E_{\perp} is the source of the large error in the VA scheme. The charge correction δK_{\parallel} corrects this error. With higher resolutions, however, the error of the volume averaged dynamic response $\langle J \rangle$ becomes larger and needs to be compensated by δJ_{\perp} .

Finally, we compare the computational cost (memory and processing time) for the different schemes. The results are summarized in Fig. 8. The staircasing scheme only requires the static epsilon ϵ_{∞} at each Yee-cell position of the E -field and the three vectorial fields E , H , J_1 . The VA algorithm additionally stores the filling factors f_1 at each Yee-cell position of the E -field. The VA+CC scheme is identical to the VA scheme for non-interface cells requiring 15 scalar components. At interface cells the VA+CC scheme requires an additional 7 scalar components for storing ρ , $J_1[\rho]$, n , f_1 and $\epsilon_{\infty,1/2}$. The comparison of computation time indicates an almost identical performance for the staircase and VA schemes. VA+CC delivers the same performance for volume cells but requires additional computational steps for interface cells, resulting in $\approx 50\%$ overhead in the per cell processing time. A 50% increase in per cell memory and processing time seems significant but rarely matters for practical applications

	Staircase	VA	VA+CC
fields (YG)	$\mathbf{E}, \mathbf{H}, \mathbf{J}_1$	$\mathbf{E}, \mathbf{H}, \mathbf{J}_1$	$\mathbf{E}, \mathbf{H}, \mathbf{J}_1$
	ϵ_∞	$\langle \epsilon_\infty \rangle, f_1$	$\langle \epsilon_\infty \rangle, f_1$
fields (CG)	-	-	$\rho, \mathbf{J}_1[\rho]$
	-	-	$\mathbf{n}, f_1, \epsilon_{\infty,1/2}$
storage/cell	12	15	15+7
time/cell	1.67	1.67	1.67+0.83

Figure 8. Computational cost (memory and CPU) of staircasing, VA and VA+CC FDTD algorithms. The various fields and parameters are either assigned to cell-centered (CG) positions or to the Yee-grid (YG). VA+CC requires same storage as VA for volume cells but carries an overhead of ~50% for interface cells. The per-cell storage values are given in QWORDS, the per-cell time in microseconds.

as the surface to volume ratio is typically small. For the Mie scattering simulations presented in Fig. 5 for example (8 cells per radius) the increase in computation time of the VA+CC algorithm is $< 1\%$ (compared to VA) as the interface/volume cell ratio is $\approx 0.6\%$.

V. CONCLUSION

In summary we presented an effective-medium theory that takes a corrective approach to the cell-averaged Maxwell's curl equations. The theory holds for static and linear dispersive permittivities and captures the field discontinuities inside a cell in form of surface current corrections, which can be calculated by integrating a surface charge equation alongside the volume-averaged curl equations. We derived a computationally efficient FDTD algorithm that allows deploying a Yee-centered stencil across the domain followed by surface current corrections that apply to interface cells. The improvement in accuracy is quantified by calculating spectral scattering cross-sections of strongly dispersive Mie scatterers. The extracted error exponents indicate that the algorithm approximately restores second order accuracy. The work presented is relevant in the current context of nano-photonic research and may pave the way to the development of novel perturbative techniques for solving Maxwell's equations.

We acknowledge useful discussions with Andrew Horsefield. This work was supported by the Leverhulme Trust and the UK Engineering and Physical Sciences Research Council.

REFERENCES

- [1] K. Yee, "Numerical solution of initial boundary value problems involving maxwell's equations in isotropic media," *IEEE Trans. Antennas Propagat.*, vol. 14, no. 3, pp. 302–307, May 1966.
- [2] A. Taflov and S. C. Hagness, *Computational Electrodynamics: The Finite-Difference Time-Domain Method*, 2005.
- [3] K.-P. Hwang and A. Cangellaris, "Effective permittivities for second-order accurate ftd equations at dielectric interfaces," *IEEE Microw. Wireless Compon. Lett.*, vol. 11, no. 4, pp. 158–160, Apr. 2001.
- [4] W. Yu and R. Mittra, "A conformal finite difference time domain technique for modeling curved dielectric surfaces," *IEEE Microw. Wireless Compon. Lett.*, vol. 11, no. 1, pp. 25–27, Jan. 2001.
- [5] M. Marcysiak and W. K. Gwarek, "Higher-order modelling of media interfaces for enhanced ftd analysis of microwave circuits," in *24th European Microwave Conf. 1994*, vol. 2, Sep. 1994, pp. 1530–1535.
- [6] N. Kaneda, B. Houshmand, and T. Itoh, "Ftd analysis of dielectric resonators with curved surfaces," *IEEE Trans. Microw. Theory Tech.*, vol. 45, no. 9, pp. 1645–1649, Sep. 1997.

- [7] M. Fujii, D. Lukashevich, I. Sakagami, and P. Russer, "Convergence of ftd and wavelet-collocation modeling of curved dielectric interface with the effective dielectric constant technique," *IEEE Microw. Wireless Compon. Lett.*, vol. 13, no. 11, pp. 469–471, Nov. 2003.
- [8] T. Hirono, Y. Shibata, W. Lui, S. Seki, and Y. Yoshikuni, "The second-order condition for the dielectric interface orthogonal to the yee-lattice axis in the ftd scheme," *IEEE Microw. and Guided Wave Lett.*, vol. 10, no. 9, pp. 359–361, Sep. 2000.
- [9] A. Mohammadi, H. Nadgaran, and M. Agio, "Contour-path effective permittivities for the two-dimensional finite-difference time-domain method," *Opt. Express*, vol. 13, no. 25, pp. 10 367–10 381, Dec. 2005.
- [10] A. Farjadpour, D. Roundy, A. Rodriguez, M. Ibanescu, P. Bermel, J. D. Joannopoulos, S. G. Johnson, and G. Burr, "Improving accuracy by subpixel smoothing in FDTD," *Opt. Lett.*, vol. 31, pp. 2972–2974, Oct. 2006.
- [11] A. Deinega and I. Valuev, "Subpixel smoothing for conductive and dispersive media in the finite-difference time-domain method," *Opt. Lett.*, vol. 32, no. 23, pp. 3429–3431, Dec. 2007.
- [12] J. Liu, M. Brio, and J. V. Moloney, "Subpixel smoothing finite-difference time-domain method for material interface between dielectric and dispersive media," *Opt. Lett.*, vol. 37, no. 22, pp. 4802–4804, Nov. 2012.
- [13] D. Kelley and R. Luebbers, "Piecewise linear recursive convolution for dispersive media using ftd," *IEEE Trans. Antennas Propagat.*, vol. 44, no. 6, pp. 792–797, Jun. 1996.



structures.

Dr. Joachim Hamm is a Leverhulme research fellow for Plasmonics and Metamaterials at Imperial College London. He did his PhD at the German Aerospace Centre (DLR), where he designed and implemented parallel software on supercomputers targeting the efficient microscopic modelling of vertical cavity surface emitting lasers (VCSELs). His research interests focus on the investigation of functional (active and nonlinear) metamaterial design, extreme light-matter interaction on the nanoscale and the stopping and localisation of light in solid-state



Fabian Renn received his diploma degree from the University of Heidelberg, Germany in 2010, followed by an Msc degree from Imperial College London in 2011. Currently, he is a PhD student within the group of Prof. O. Hess at Imperial College London. His research interests include numerical simulation techniques of light matter interactions. His diploma thesis focused on theory and simulation of x-rays interacting with patterned strained silicon germanium at AMD Dresden, Germany.



Prof. Ortwin Hess holds the Leverhulme Chair in Metamaterials in the Department of Physics at Imperial College London and is Co-Director of the Centre for Plasmonics & Metamaterials. Ortwin studied physics at the University of Erlangen and the Technical University of Berlin. Ortwin has been (from 1995 to 2003) Head of the Theoretical Quantum Electronics Group at the Institute of Technical Physics in Stuttgart, Germany. Since 2001 he is Docent of Photonics at Tampere University of Technology in Finland. Ortwin has been Visiting Professor at Stanford University (1997 - 1998) and the University of Munich (2000 - 2001). From 2003-2010 he held the Chair of Theoretical Condensed Matter and Optical Physics in the Department of Physics and the Advanced Technology Institute at the University of Surrey in Guildford, UK where he is now a Visiting Professor.